Thin Solid Films 710 (2020) 138268

Contents lists available at ScienceDirect

Thin Solid Films

journal homepage: www.elsevier.com/locate/tsf

Mechanical properties of homogeneous and nitrogen graded TiN thin films

Felipe C. Silva[a,b], Matheus A. Tunes[c], Julio C. Sagás[d], Luis C. Fontana[d], Nelson B. de Lima[e], Cláudio G. Schön[*,a]

[a] Department of Metallurgical and Materials Engineering, Escola Politécnica da Universidade de São Paulo, Av. Prof. Mello Moraes, 2463, São Paulo-SP 05508-900, Brazil
[b] Faculdade de Tecnologia de Cotia, Centro Estadual de Educação Tecnológica "Paula Souza", Rua Nelson Raineri, 700, Cotia – SP 06702-155, Brazil
[c] Chair of Non-Ferrous Metallurgy, Montanuniversitaet Leoben, Franz-Josef-Strasse 18, Leoben 8700, Austria
[d] Laboratory of Plasmas, Films and Surfaces, Universidade do Estado de Santa Catarina, Rua Paulo Malschitzki, 200 – Zona Industrial Norte, Joinville-SC, 89219-710, Brazil
[e] Centro de Ciências e Tecnologia dos Materiais, Instituto de Pesquisas Energéticas e Nucleares, Comissão Nacional de Energia Nuclear em São Paulo, Av. Prof. Lineu Prestes, 2242 - Butantã, São Paulo - SP, 05508-000, Brazil

ARTICLE INFO

Keywords:
Characterization
Fracture behavior
Stress measurements
X-ray analysis
Ceramics
Coatings

ABSTRACT

Coating of metallic industrial parts with titanium nitride (TiN) is widely used with the aim to improve the mechanical and tribological properties of these parts. In the present work, TiN films were deposited via grid-assisted magnetron sputtering on aluminium substrates. The films were grown under different substrate bias voltage (-40, -75 or -100 V) and two different modes of nitrogen supply during deposition (constant and variable), resulting in homogeneous and N-graded films. The results of tension fractures observed *in situ* were correlated with the film microstructure and residual stress levels obtained through grazing incidence X-ray diffraction measurements. Elastic properties of the films were analysed via nanoindentation and adhesive properties were investigated by nanoscratching tests. Results show that the delamination load of the graded films is higher than in the homogeneous counterparts, suggesting the graded film have improved tribological properties.

1. Introduction

The durability of the industrial parts is significantly improved by the deposition of a coating with high hardness [1]. Among the most common coatings used for cutting tools, thin films based on titanium nitride (TiN) are highlighted [2–7]. TiN coatings are also largely used in the automotive, aerospace, microelectronics and even in sanitary industries. Besides the high hardness, such films present high corrosion resistance, and excellent mechanical, electrical, and optical properties [8–12]. Recently the use of TiN thin films has been suggested even for nuclear applications, to protect Zircaloy fuel claddings from oxidation by steam in the event of a severe accidents[13,14], unfortunately the radiation damage tolerance in these films seems to be insufficient [15,16].

Physical vapor deposition techniques (PVD) are commonly used for obtaining TiN thin films [17]. The magnetron sputtering technique, in particular, has the advantage of using low deposition temperatures and enhanced control of thickness and pressure, resulting in more homogeneous thin films [18]. Grid-assisted magnetron sputtering (GAMS) is an evolution of the conventional magnetron sputtering technique [19,20]. In this configuration, a grid is inserted between the sputtering target and the substrate, allowing a better confinement of the produced plasma [21–24]. As a consequence, it is possible to deposit the film at lower pressures, which results in more compact films [19,20]. Besides that, the grid reduces the effective gettering area, reducing the hysteresis in reactive sputtering [20,25]. The GAMS technique also allows the alteration of additional process parameters such as the substrate bias and N_2 flow rate during film growth.The substrate bias controls the energy of the ions impinging at the film surface. It has the known effect of inducing residual stresses in the plane of the film. These (compressive) stresses can reach values around of –10 GPa [26–28]. Variable N_2 flow rate induces a nitrogen gradient along the film thickness (N-graded TiN film)[29], allowing obtain functionally graded films.

The aim of the present work is to study the effect of different values of substrate bias on both mechanical and adhesive performances of N-graded TiN films deposited onto AA1000 substrates by using the GAMS technique. These will be compared with homogeneous TiN films produced under similar conditions.

* Corresponding author.
E-mail addresses: felipecarneiro@usp.br (F.C. Silva), schoen@usp.br (C.G. Schön).

https://doi.org/10.1016/j.tsf.2020.138268
Received 2 May 2020; Received in revised form 4 August 2020; Accepted 4 August 2020
Available online 07 August 2020
0040-6090/

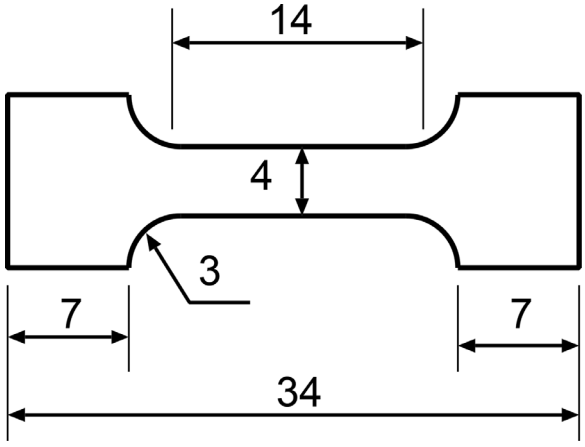

Fig. 1. Geometry of the aluminium substrates. Dimensions in mm.

2. Methodology

2.1. Materials

TiN films were deposited onto 3 mm thick AA1100 aluminium substrates, prepared in the geometry of a "dog-bone" type tensile sample, whose dimensions are represented in Fig. 1. The choice of substrate material was due to its smaller Young modulus compared with steels and nickel superalloys. By this, the occurrence of failures in the film are more probable, since a larger elastic strain is sustained in the substrate for smaller loads.

A surface like a mirror of the substrates before deposition was prepared by grinding with SiC paper up to #2000 mesh and then polishing using 1 μm diamond paste. All the substrates were ultrasonic cleaned in tetrachloroethylene for 10 min prior to deposition.

The GAMS chamber is made of stainless steel (internal diameter: 30 cm, height: 25 cm). The vacuum system is composed by mechanical and turbomolecular pumps. The Ti sputtering target (99.5% pure) has 100 mm in diameter and 5 mm thick. The magnetron is unbalanced of type II. The grid (mesh 1 × 1 mm) is grounded and works as the discharge anode. The grid-to-target distance was fixed at 20 mm. The grid was made of austenitic stainless steel in order to avoid distortions of magnetic field lines. The substrate holder was 60 mm away from the target. It has 100 mm in diameter and is made of Cu. Prior deposition, the chamber was evacuated to a pressure around 10^{-2} Pa and the target surface was sputter cleaned.Depositions were carried out in an atmosphere of Ar (99.999%) and N_2 (99.999%). The plasma was generated by a Pinnacle Plus power supply operating in direct constant current mode. The discharge current was fixed at 2 A, corresponding to a target power density around 13 W/cm^2. In all depositions, the total pressure was kept at 0.40 Pa according a capacitive gauge. The substrates were heated up to 573 K by a set of halogen lamps and the substrate temperature was monitored by a type K thermocouple. The working gases flow rates were adjusted using mass flow controllers (20 sccm full scale). For each film, a 150 nm thick Ti interlayer was deposited before the TiN_x deposition to improve film adhesion[28,30–32]. All depositions lasted 30 min. Two conditions of N_2 supply were used: constant (homogeneous film) and variable (graded film). For the homogeneous films, the N_2 flow rate was maintained constant around 8.0 sccm, close to the first critical point, but before target positioning [33]. For the graded films, the N_2 flow rate was set initially to 1.5 sccm, being increased in steps of 0.4 sccm/min until around 8.0 sccm. Then the N_2 flow rate was maintained constant during the last 15 minutes of deposition. For both cases (homogeneous and graded films), three conditions of substrate bias voltage were used: -40 V, -75 V and -100 V.

In a previous publication [29], the thickness and cross section of the TiN films (homogeneous and graded) were obtained by scanning electron microscopy (SEM). These results showed that the films have thickness from 1.0 to 1.5 μm and columnar structure.

2.2. Film characterization

2.2.1. Residual stresses

X-ray diffraction was performed in the Grazing Incidence mode (GIXRD) using a Rigaku Multiflex diffractometer, in the $\theta - 2\theta$ configuration, using a scanning range of $25^o \leq 2\theta \leq 80^o$, with a step of 0.02ºand 6 s acquisition time per step. Cu Kα radiation (λ= 0.15406 nm) was employed for the experiments, in order to determine the residual stress levels induced in the film plane. An attempt of using the technique for the graded films proved unsuccessful, probably because both the stress levels and the lattice parameter of TiN are thickness-dependent, due to the gradient in nitrogen concentration. The developed stresses are supposed to be approximately equivalent in the homogeneous and graded films, at least in the order of magnitude, and in the qualitative intensity. The residual stresses were obtained using the $\sin^2\phi$ method [34]. The GIXRD experiments were performed using incidence angles of 3, 7,10, 12 and 15º.

2.2.2. Tensile test

Tensile tests were performed in a custom-made testing machine, which consists of a motor-driven axle containing a right-hand thread on one side and a left-hand thread on the other side, so that the sample can be strained while its center-of-mass remains static. The machine contains an attached microscope, which allows to observe *in situ* the development of cracks in the central portion of the sample during the test. The machine has a capacity of 10 kN measured through a calibrated load cell and the tests were developed at 0.1 mm/min displacement rate. Strains are measured via the displacement of the grips, but since both loads and sample stiffness are small, a correction due to machine stiffness can be neglected.

2.2.3. Mechanical properties

The mechanical characterization was further performed using instrumented indentation with a Hysitron TI 950 Triboindenter with a Berkovich tip and 5 mN load, using the procedure suggested Pharr *et al.* [35]. The indentations were performed using 5 s for the loading time, 2 s holding time, and 5 s for unloading time.

Hardness, H, is defined as:

$$H = \frac{P_{max}}{A_{max}} \tag{1}$$

where $P_{\max}$ and $A_{\max} = A(h_{\max})$ are defined as the load and contact areas at maximum load.

Young modulus can be determined in the form of a reduced modulus, E_r, through the modified Sneddon's equation[35]:

$$\left.\frac{\partial P_u}{\partial h}\right|_{h_{max}} = \beta\frac{2}{\sqrt{\pi}}\sqrt{A}\,E_r \tag{2}$$

In the expression, $P_u(h)$ represents the unloading portion of the load-displacement curve and β is a form factor correction for the indenter geometry in which for the Berkovitch indenter, takes the value $\beta = 1.034$ [35].

Herein, the load applied in the present experiments was observed to produce maximum displacements below 10% of the film thickness, so that the results are unaffected by the presence of the substrate.

2.2.4. Scratching tests

Scratching tests were performed using a CETR microtribometer (model UMT-2), with 1 N pre-load and progressive load mode. For this experiment a 120º spheroconical diamond indenter was employed. In these experiments, load was progressively increased until a trail of about 3 mm was produced. The indenter displacement speed was set to

10 mm min^{-1}. The test was evaluated in the form of the load corresponding to the observation of the first cracks (denoted Lc1, associated with a cohesive failure of the film) and the load corresponding to the observation of delamination (denoted Lc2, corresponding to an adhesive failure).

3. Results and discussion

This section presents statistical analysis data to analyze the experimental results.The uncertainty of all experimental results will be discuss referred to using Students t Distribution [36]. The sources of error in the present measurements are assumed to be statistically independent, therefore it is reasonable to assume that these measurements are described by normal distributions with the average, μ, and standard deviation, σ, estimated from the measurements. Furthermore, it is possible to assume that the sources of error are also independent from the variation of process parameters (both the employed bias and nitrogen flow mode), therefore it is also reasonable to assume that the different measurements are described by distributions with equal variances, σ^2.

Students t Distribution allows us to perform a complete statistical analysis, evaluate the null hypothesis of equality between means, m_1 and m_2 obtained in two experiments with n measurements each. The present analysis is limited to the case in which the number of samples is the same for the two measurements: the case of "paired samples".As usual this is done by considering the stocastic variable t, defined as:

$$t = \frac{(m_1 - m_2)}{s_P\sqrt{\frac{2}{n}}} \tag{3}$$

in this expression, s_P is the square root of the so-called "pooled variance", which is an estimator of the true variance of the population. This can be obtained from the standard deviations s_1 and s_2, obtained in the measurements, as:

$$s_P^2 = \frac{(n-1)(s_1^2 + s_2^2)}{(2n-2)} \tag{4}$$

Under the present hypotheses, the stocastic variable t follows a (central) T^{2n-2} distribution with $(2n-2)$ degrees-of-freedom. By choosing a given significance level α, the method allows to determine whether the difference between the averages m_1 and m_2 are significant or not, by comparing the variable t (measured) with the argument of T_α^{2n-2} which forms the interval $[-T_\alpha^{2n-2}, T_\alpha^{2n-2}]$ which corresponds to an accumulated probability $1-\alpha$. In this sense, α corresponds to the probability of the Type I error: rejecting the null hypothesis when it should be accepted.In case the hypothesis of equality between the averages is not rejected, another possible statistical error is defined, which is known as "type II error" (accepting the hypothesis when it should be rejected), this defines β. This is defined as (for the two-tailed analysis):

$$\beta = F_\delta^{(2n-2)}(t) - F_\delta^{(2n-2)}(-t) \tag{5}$$

where F represents the accumulated distribution function of the non-central T distribution [37] with $(2n-2)$ degrees-of-freedom and non-centrality parameter δ, defined as:

$$\delta = \left(\frac{m_1 - m_2}{\sigma_P}\right)\sqrt{\frac{n}{2}} \tag{6}$$

In case a single-tailed analysis is necessary, only the first term in the summation of the right hand side of Eq. (5) is preserved. The power of the statistical test is defined a $1-\beta$.The analysis is made by first defining whether the difference of two measurements is signficant or not (by setting a value of $\alpha = 0.05$, defining whether the null hypothesis should be rejected or not). In case the null hypothesis is not rejected, the power is used in the discussion.

Table 1
Residual stresses (in GPa) determined in the GIXRD experiments for the homogeneous films.

Reflection	−40 V	-75 V	-100 V
(111)	−6.3	−8.0	−6.9
(200)	−6.9	−5.9	−9.8
(220)	−4.5	−4.1	−7.8
Average	−5.9 ± 1.2	−6.0 ± 2.0	−8.2 ± 1.5

3.1. GIXRD

3.1.1. Experimental results

Table 1 shows the residual stresses determined in the homogeneous films by GIXRD. Compressive residual stresses are induced in the film, independent of the applied bias. Increasing the substrate bias leads to the nominal increase of the average compressive residual stress, from approximately –5.9 to –8.2 GPa. However, due to the large uncertainties, they must be considered constant since, according to the t-Student test (Table 2), none of the three possible combinations of measurements allows to reject the null hypothesis under 95% confidence. When the power of the tests are compared, however, we observe that accepting the null hypothesis when comparing the –40 V and –75 V bias cases has 94.4% probability of being the correct choice, but not for the comparisons between –40 V and –100 V (41.7%) and between –75 V and –100 V (54.2%). Considering that an increase in residual stress is expected due to physical arguments, this shows us that the increase is real and cannot be statistically attested just due to the small number of measurements, which are limited due to the accessibility of the instrument.

Figure2 shows GIXRD patterns for homogeneous (Figure2 a) and graded (Figure2 b) TiN films, using incidence angle of 15º. The labeled peaks corresponds to cubic TiN crystallographic planes. It is observed that the TiN peaks for graded films are considerably broader, which is a consequence of the nitrogen gradient along the thickness [29]. This results in different lattice parameters of the film along the thickness, and since the GIXRD technique probes different thicknesses with different incidence angles, this effect cannot be separated from the lattice parameter variation due to the residual stresses. The residual stresses in the graded films cannot be determined, however, apart from the variations of Young modulus which is expected due to the variation of nitrogen content, it is assumed this will introduce only a small perturbation compared with the homogeneous films, therefore it is concluded that different bias levels introduce compressive residual stresses in both film configurations, which are of the order of GPa, furthermore, it is concluded that the higher the bias is, the more intense are the residual stresses.

As already reported [29], for the homogeneous films the most intense peak is (200) suggesting the preferred orientation is (001) along the thickness direction. For the graded films, the most intense peak is (111). It is suggested that the variation of N_2 supply during film growth introduces a directional factor which leads to a different growth mode, thus changing the preferred orientation. It is probably related to the variation of N/Ti atom flux to the substrate during gradual N_2 flow rate increase during the deposition of graded films [38].

3.1.2. Statistical analysis

Table 2 shows the analysis of the residuals stresses determined in the homogeneous (H) films using Grazing – Incidence X-ray Diffraction (the graded samples will be identified as "G" throughout the present document).

As the analysis shows, the results support the conclusion that the residual stress levels are not influenced by the bias, but the low values of power for the comparisons with the –100 V case suggest that the influence is not detected only because of the small number of samples

Table 2
Statistical analysis for the residual stress levels as a function of the bias.

Comparison	Av1	Va1	Av2	Va2	n	t	$T_{0.05}^{2n-2}$	δ	$\beta = F_{\delta}^{2n-2}(t)$	1-β
H (−40 V/ −75 V)	−5.9	1.44	−6	4	3	0.074	2.776	0.0612	0.055	**0.945**
H (−75 V/ −100 V)	−6	4	−8.2	2.25	3	1.524	2.776	1.232	0.458	**0.542**
H (−40 V/ −100 V)	−5.9	1.44	−8.2	2.25	3	2.074	2.776	1.669	0.583	**0.417**

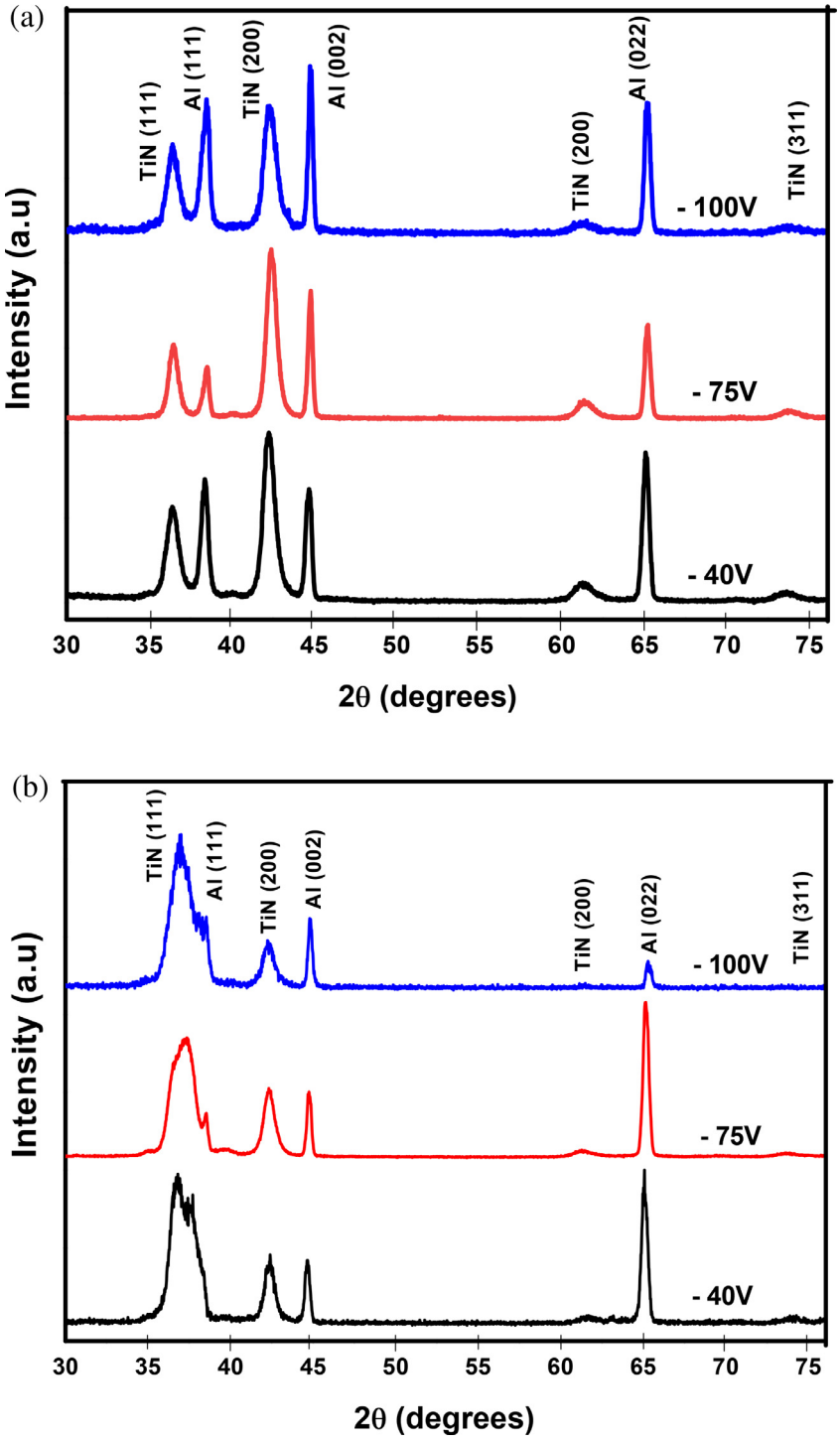

Fig. 2. GIXRD patterns obtained at 15° grazing angle for all investigated bias: (a) homogeneous films, (b) graded films.

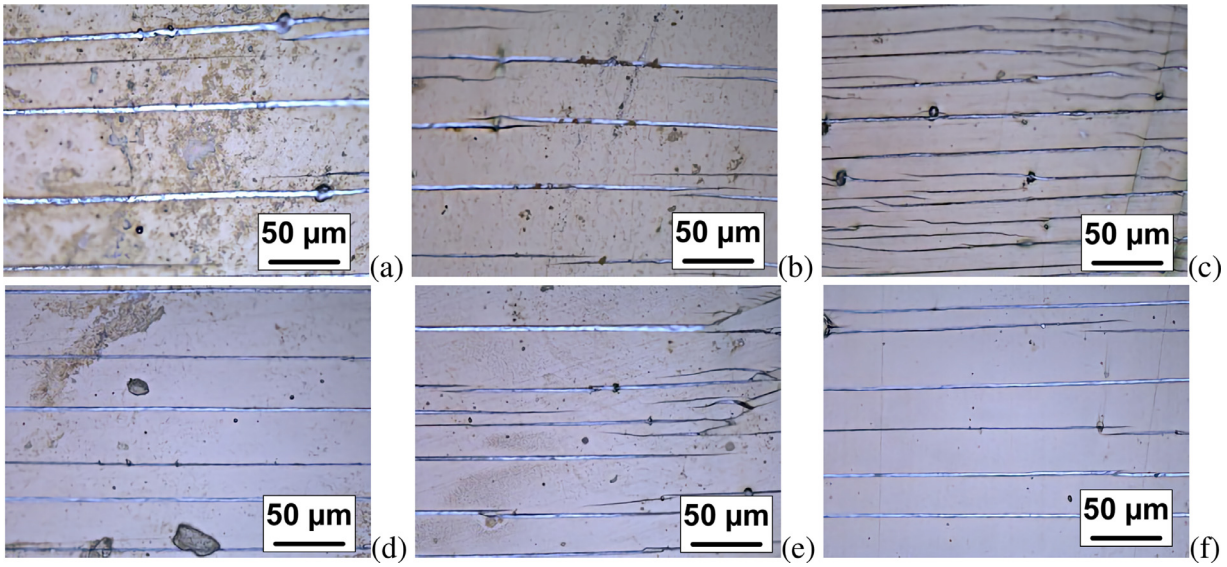

Fig. 3. Saturation distance configuration observed for the film cracks in the tensile tests. (a) Homogeneous, –40 V bias, (b) Homogeneous, –75 V bias, (c) Homogeneous, –100 V bias, (d) Graded, –40 V bias, (e) Graded, –75 V bias, (f) Graded, –100 V bias.

investigated. In this table, and in the other contained in the present document, Av1 and Av2 represent the two averages being compared, Va1 and Va2 represent the respective variances, n is the number of measurements used to calculate the averages (and variances), t is the calculated value for the stochastic variable in the t-Student test, $T_{0.05}^{2n-2}$ is the critical two-tailed argument of the T distribution corresponding to an α= 0.05 probability for the Type I error (rejecting the null hypothesis, when it should in fact be accepted). If the comparison is made using the single-tailed test, to show for example that the values are significantly larger of smaller, the same critical value can be used, corresponding then to $\alpha = 0.025$. In this table, δ represents the non-centrality parameter used in the non-central T distribution and $F_{\delta}^{2n-2}(t)$ is the accumulated probability distribution for the non-central T distribution, with non-centrality parameter δ and degrees-of-freedom $2n - 2$. Finally $1 - \beta$ corresponds to the power of the test, where β is the probability of the Type II error (accepting the null hypothesis when it should in fact be rejected).

The comparisons in which the null hypothesis is rejected will be presented by highlighting (**in bold text**) the t value, otherwise the power $(1 - \beta)$ is highlighted. In this way a visual appreciation of the results is possible at which the relevant statistical parameter is noted.

3.2. Tensile tests

3.2.1. Experimental results

Fig. 3 shows the final configuration of the deposited films. The test was stopped after no further cracks were detected in the field of view of the stereo-microscope, indicating that crack separation saturated at the lowest average distance (the critical distance). Comparison with similar cracks produced in identical films deposited over brass, with significantly smaller crack saturation distances, validated the hypothesis that using a low stiffness substrate leads to better control of film cracking [39].

This case is similar to fiber reinforced composites where the saturation distance, λ_{sat}, is determined by the equilibrium between the fracture strength of the fiber and the load transfer capacity of the interface with the matrix [40,41]. The formalism for thin film systems has been already developed in the literature [42,43], including the effect of "in plane" residual stresses. In this formalism, the critical interface shear strenght, τ_c, is defined as:

$$\tau_c = \frac{\pi \sigma_f t_f}{\lambda_{sat}} \tag{7}$$

where t_f is the film thickness, which is assumed to be 2 μm [29] for both films, and σ_f is the fracture strength of the film, estimated by:

$$\sigma_f = E\varepsilon_f + \sigma_{res} \tag{8}$$

with ε_f being the macroscopic strain of the sample in which the first crack is observed during the test, σ_{res} represents the compressive residual stress in the film, $E = 241$ GPa being adopted as the Young modulus of the TiN film, using the values estimated in the nanoindentation experiments (Section 3.3) and solving for E in Hertz equation [35,44]:

$$\frac{1}{E_r} = \frac{1 - \nu_{\mathrm{TiN}}^2}{E} + \frac{1 - \nu_{\mathrm{Diamond}}^2}{E_{\mathrm{Diamond}}} \tag{9}$$

using published values of the diamond indenter's Young modulus ($E_{\mathrm{Diamond}} = 1140$ GPa) and Poisson's coefficient ($\nu_{\mathrm{Diamond}} = 0.07$)[44], and of Poisson's coefficient for TiN ($\nu_{\mathrm{TiN}} = 0.19$) [45].

As discussed in Section 3.1, the residual stresses could not be determined in the graded films, we assume as a first approximation that they are identical as the ones observed in the corresponding homogeneous films for the same bias levels.Table 3 shows the average distance between cracks for all deposition conditions. The results confirm the qualitative analysis of the images show in Fig. 3.

Comparing first the averages of λ_{sat} for the homogeneous and graded films, we observe that statistical significant differences are observed only for the cases of –75 V and – 100 V bias (Table 4). The conclusion about difference for the case of – 40 V bias, although not statistical significant, has a power of 58.3%. The graded film, therefore,

Table 3
Critical distances measured for the deposited films in all parameter configurations (the uncertainties are determined as the standard deviation of the measurements).

Configuration	λ_{sat} [μm]	ε_f	τ_c [GPa]
Homogeneous, –40 V bias	36.9 ± 4.5	0.18 ± 0.05	6.5 ± 2.6
Homogeneous, –75 V bias	31.0 ± 2.1	0.20 ± 0.04	6.4 ± 2.8
Homogeneous,–100 V bias	21.6 ± 1.0	0.10 ± 0.04	7.2 ± 2.8
Graded, –40 V bias	32.9 ± 8.6	0.10 ± 0.03	4.8 ± 0.8
Graded, –75 V bias	35.1 ± 0.5	0.12 ± 0.01	3.8 ± 0.1
Graded,–100 V bias	35.9 ± 3.4	0.10 ± 0.02	5.1 ± 0.5

Table 4
Statistical analysis for the minimum distance between cracks in the tensile tests (λ_{sat}) both as a function of deposition mode and of the bias.

Comparison	Av1	Va1	Av2	Va2	n	t	$T_{0.05}^{2n-2}$	δ	$\beta = F_{\delta}^{2n-2}(t)$	1-β
−40 V (H/G)	36.9	20.3	32.9	74.0	3	0.714	2.776	0.598	0.417	**0.583**
−75 V (H/G)	31.0	4.4	35.1	0.3	3	**−3.289**	2.776	3.090	0.489	0.511
−100 V (H/G)	21.6	1.0	35.9	11.6	3	**−6.989**	2.776	6.369	0.509	0.491
H (−40 V/ −75 V)	36.9	20.3	31.0	4.41	3	2.058	2.776	1.752	0.554	**0.446**
H (−75 V/ −100 V)	31.0	4.4	21.6	1.0	3	**7.000**	2.776	5.942	0.576	0.424
H (−40 V/ −100 V)	36.9	20.3	21.6	1.0	3	**5.749**	2.776	5.451	0.472	0.528
G (−40 V/ −75 V)	32.9	74.0	35.1	0.3	3	−0.442	2.776	0.474	0.286	**0.714**
G (−75 V/ −100 V)	35.1	0.3	35.9	11.6	3	−0.403	2.776	0.402	0.269	**0.731**
G (−40 V/ −100 V)	32.9	73.9	35.9	11.6	3	−0.562	2.776	0.490	0.355	**0.645**

shows larger λ_{sat} compared with the corresponding homogeneous films.

Comparing now the λ_{sat} averages for films produced with different values of bias (Table 4), we observe that in the case of the homogeneous films only the comparison between bias –40 V and –75 V does not show a significant difference (with power 44.6%), this leads to the conclusion that increasing bias results in decreasing λ_{sat}. However, in the case of graded films the comparison of average differences in any two combination of bias is not statistically significant, and the comparison between –40 V and –75V results in a power of 71.4%, the comparison of –40 V and –100 V shows a power of 64.5%, and the comparison between –75 V and –100 V results in a power of 73.1%. In the case of the graded films, therefore, it is concluded that there is no effect of bias on λ_{sat}.

When comparing the critical interfacial shear strength, however, different sources of error combine and the calculated critical shear strengths become independent of the bias. In the case of the homogeneous films this conclusion is very robust, since the calculated powers (Table 5) are very large (96.6% for the comparison between –40 V and –75 V, 97.4% for the comparison between –75 V and –100 V and 77.4% in the comparison between –40 V and –100 V). In the case of the graded films the critical interface shear stresses are also not affected by the bias, however the difference between the –75 V and –100 V cases is statistically significant (Table 5). This is probably due to the unusually small value of standard deviation measured for the –75 V case. The standard deviation is also a stochastic variable therefore it is also affected by statistical uncertainty, so this low value of standard deviation can be misleading.

The interfaces are expected to be affected by the bias, but apparently this effect is small leading to a constant critical interface shear strength. The average differences comparing case by case the three bias values are not statistically significant, with low values of power (51.7% in the case of –40 V, 59% in the case of –75 V, and 53% in the case of –100 V). Since the values were considered independent of bias, a general average of the nine measurements in each condition can be made, resulting in $\tau_c = 6.7 \pm 2.3$ GPa in the homogeneous film and $\tau_c = 4.6 \pm 0.7$ GPa for the graded film, this difference is statistically significant and shows that the critical shear stress in the graded film is significantly smaller than the one measured for the homogeneous film.

3.2.2. Statistical analysis

Table 4 shows the results for the statistical analysis concerning the saturated minimum distance between cracks, observed in the tensile tests. In this case, comparisons can be made for samples obtained with different deposition modes using the same value of bias, and for a given deposition mode, between samples obtained with different bias values.

The analysis of the results show that the graded samples are characterized by significantly larger values of λ_{sat} for bias value of –75 V and –100 V. The null hypothesis cannot be rejected for the –40 V bias cases, but this conclusion is characterized by a small value of power (58.3%), so the analysis is inconclusive in this case. In the cases of –75 V and –100 V bias, the results show that λ_{sat} is increased, so in these cases the single-tailed test can be used and shows that this increase is significant for an $\alpha = 0.025$ level.

Comparing samples obtained with different deposition modes, it is observed that for the homogeneous samples, increasing the bias to –100 V leads to higher values of λ_{sat}. The null hypothesis cannot be rejected for the – 40 V and – 75 V cases, but this is characterized by a small power, showing that this conclusion is rather weak. In the case of the graded samples all three comparisons show that the effect of bias is not detected and this is followed by slightly larger values of power, increasing the confidence in this conclusion.

Table 5 compares the critical interface shear strengths derived from the λ_{sat}, ε_f and residuals stress measurements for the deposition mode (given a value of bias) and for different bias in the same deposition mode. Most comparisons result in accepting the null hypothesis, except for the comparison between −75 V and – 100 V bias in the graded samples. As discussed in the main manuscript, the variance of the –75 V graded samples is suspiciously small. The results suggest, therefore that the critical interface shear strength is independent of the bias. Using this hypothesis, general averages (and variances) can be calculated for the nine samples corresponding to each deposition mode, and this is shown in the last line of the table. These averages show that the critical interface shear strength of the graded samples is significantly smaller in the graded samples, compared with the homogeneous samples. Since this is a single-tailed test, the α value used in this comparison is 0.025.

Table 5
Statistical analysis for the critical interface shear strength (τ_c) both as a function of deposition mode and of the bias.

Comparison	Av1	Va1	Av2	Va2	n	t	$T_{0.05}^{2n-2}$	δ	$\beta = F_{\delta}^{2n-2}(t)$	1-β
−40 V (H/G)	6.5	6.76	4.8	0.64	3	0.045	2.776	0.980	0.483	**0.517**
−75 V (H/G)	6.4	7.84	3.8	0.01	3	−0.350	2.776	1.757	0.410	**0.590**
−100 V (H/G)	7.2	7.84	5.1	0.25	3	−0.317	2.776	1.247	0.470	**0.530**
H (−40 V/ −75 V)	6.5	6.76	6.4	7.84	3	0.045	2.776	0.036	0.034	**0.966**
H (−75 V/ −100 V)	6.4	7.84	7.2	7.84	3	−0.350	2.776	0.280	0.025	**0.975**
H (−40 V/ −100 V)	6.5	6.76	7.2	7.84	3	−0.317	2.776	0.254	0.226	**0.774**
G (−40 V/ −75 V)	4.8	0.64	3.8	0.01	3	2.148	2.776	2.177	0.444	**0.556**
G (−75 V/ −100 V)	3.8	0.01	5.1	0.25	3	**−4.416**	2.776	4.246	0.463	0.537
G (−40 V/ −100 V)	4.8	0.64	5.1	0.25	3	−0.551	2.776	0.452	0.355	**0.645**
H/G	6.70	5.06	4.57	0.55	9	**2.702**	2.120	2.265	0.539	0.461

Table 6
Results from the nanoindentation tests (uncertainties are estimated as the standard deviation of the measurements).

Condition	E_r [GPa]	H [GPa]	γ [GPa]
Homogeneous, –40 V bias	207.1 ± 4.8	21.3 ± 1.0	0.23 ± 0.02
Homogeneous, –75 V bias	185.4 ± 4.8	20.1 ± 1.0	0.19 ± 0.02
Homogeneous,–100 V bias	205.4 ± 4.3	23.4 ± 1.0	0.30 ± 0.03
Graded, –40 V bias	203.2 ± 11.6	19.9 ± 2.0	0.19 ± 0.04
Graded, –75 V bias	197.5 ± 9.3	22.5 ± 1.8	0.29 ± 0.05
Graded,–100 V bias	215.9 ± 11.3	24.8 ± 2.2	0.33 ± 0.06

3.3. Nanoindentation tests

3.3.1. Experimental results

Table 6 presents the results of the reduced Young modulus of the system indenter + film, hardness and parameter γ, defined as:

$$\gamma = \frac{H^3}{(E_r)^2} \tag{10}$$

Both Young modulus and hardness show no discernible effect from bias in both conditions. A representative value of E_r =205 GPa was chosen to be used in Section 3.2, this is slightly larger than the average of all values (≈ 202 GPa), to compensate for the anomalously low value obtained in the -75 V bias case in the homogeneous film.

The process parameters have no effect over the film modulus, however the statistical uncertainty of the values definitely increased for graded films. The application of the t-Student test (Table 7) to these values leads to significant differences between all combinations, except for the comparison between the –40 V and –75 V cases in the graded films (with a power of 50%). There are, however, no discernible patterns in the variation of Young modulus for both cases. These results could be explained by the gradient of properties expected to exist along thickness. In the derivation of Sneddon's formula it is implicitly assumed that the indented material has homogeneous properties and this is strictly valid only for the homogeneous films. Therefore the observed dispersion Young modulus measured for both films must be considered with care, and are likely to be a result of other statistical errors which are not controlled in the present investigation.

Hardness shows an apparent tendency of increase with the applied bias. These variations are statistically significant considering the t-Student test (Table 8). All combinations of averages indicate that the hardness increases with the applied bias, except for the –40 V and –75 V cases in the homogeneous films, in which a decrease of hardness is detected. As observed in the discussion of the Young modulus, there is indication of sampling anomaly for the homogeneous film obtained with –75 V bias. This anomaly could affect the hardness measurements, as well. Comparing the hardness of all applied bias (–40 V,–75 V and –100 V) both homogeneous and graded films, we observe that only the case with –75 V bias results in a statistically significant increase of hardness for the graded film. This result is doubtful, due to the sampling anomaly in the homogeneous film, as already discussed.

The parameter γ (supposed to be an indicator of film toughness [46]) apparently increases with bias and is larger for the graded films (except for the –40 V bias case, in which there is a reduction). According the t-Student test (Table 9), all combinations of bias, except the one for the –75 V and –100 V cases (with a power of 49%) in the graded film, are significantly different. Also, all cases except in the comparison between –40 V and –75 V bias in the homogeneous films indicate an increase of α with increasing bias. Comparing the homogeneous and graded films, we observe that the difference is significant in all bias values, except for the result of –40 V, which indicates a reduction of the parameter. Both the results for –75 V and –100 V points at a significant increase of γ for the graded films.

3.3.2. Statistical analysis

Table 7 shows the comparisons for the averages in the determination of the Young modulus for the graded samples. As explained in the main manuscript, the results of the homogeneous samples also show different values depending on the bias, but these are disregarded and a representative value is selected, instead. The statistical analysis show that the null hypothesis (equality of averages) can be rejected for the comparisons between bias –40 V and – 100 V and – 75 V and –100 V, but not for the comparison between – 40 V and – 75 V (with a power of 50%). These results suggest that the Young modulus would be affected by the bias (increasing it) at least for the – 100 V bias, but as explained in the main manuscript, these results should be cautiously considered.

Hardness (H) values – as determined from the instrumented indentation tests – are compared with reference to deposition mode and to bias for a given deposition mode. These comparisons are shown in Table 8. The null hypothesis cannot be rejected for the case of the deposition mode (with powers around 52%), except for the – 75 V bias case in which a significant difference is detected. These results suggest that the deposition mode affects the hardness of the film, but since no pattern is apparent (hardness decreases for the – 40 V bias, and increases for – 75 V and – 100 V cases), the result should be interpreted as inconclusive. Concerning the effect of bias, in all comparisons the null hypothesis is rejected, and with the exception of the – 40 V bias case in the homogeneous sample, there is a clear indication that increasing the bias, leads to an increase in film hardness.

The analysis of the derived parameter γ is shown in Table 9. In all comparisons, except for the comparison between the homogeneous and grade films for –100 V bias, and for the graded films obtained with –75 V and –100 V bias, the null hypothesis is rejected. The cases in which the hypothesis is not rejected are characterized by very low powers (51.8% and 49% respectively). In particular, except for the cases involving the homogeneous films obtained with –40 V bias, the comparisons indicate an increase of the parameter (both with the film growth mode and of the increase with bias).

3.4. Scratch tests

3.4.1. Experimental results

Table 10 presents the results obtained in the nanoscratching tests, in the form of loads Lc1 and Lc2, associated respectively with a cohesive failure (appearance of cracks in the film) and to delamination failure.

No significant difference is observed in the values of Lc1 for the homogeneous films. In the case of the graded films the comparison between Lc1 for the –40 V and –75 V and of Lc2 for the –75 V and –100 V cases are statistically significant (Table 11). In the remaining combinations the null hypothesis (equality of the averages) is accepted, but with powers as low as 48% (comparison of Lc1 averages for the –40 V and –100 V cases in the homogeneous sample) and 42.5% (graded samples). Assuming the values of Lc1 are independent on bias,

Table 7
Statistical analysis for the reduced Young modulus as a function of the bias.

Comparison	Av1	Va1	Av2	Va2	n	t	$T_{0.05}^{2n-2}$	δ	$\beta = F_{\delta}^{2n-2}(t)$	1-β
G (−40 V/ −75 V)	203.2	134.6	197.5	86.5	10	1.212	2.101	1.168	0.500	**0.500**
G (−75 V/ −100 V)	197.5	86.5	215.9	127.7	10	**−3.976**	2.101	3.826	0.530	0.470
G (−40 V/ −100 V)	203.2	134.6	215.9	127.7	10	**−2.480**	2.101	2.376	0.525	0.475

Table 8
Statistical analysis for the hardness of the films as a function of deposition mode and of bias.

Comparison	Av1	Va1	Av2	Va2	n	t	$T_{0.05}^{2n-2}$	δ	$\beta = F_{\delta}^{2n-2}(t)$	1-β
−40 V (H/G)	21.3	1.00	19.9	4.00	10	1.980	2.101	2.000	0.478	**0.522**
−75 V (H/G)	20.1	1.00	22.5	3.24	10	**−3.686**	2.101	3.671	0.484	0.516
−100 V (H/G)	23.4	1.00	24.8	4.84	10	−1.832	2.101	1.874	0.473	**0.527**
H (−40 V/ −75 V)	21.3	1.00	20.1	1.00	10	**2.683**	2.101	2.570	0.526	0.474
H (−75 V/ −100 V)	20.1	1.00	23.4	1.00	10	**−7.379**	2.101	7.068	0.548	0.452
H (−40 V/ −100 V)	21.3	1.00	23.4	1.00	10	**−4.696**	2.101	4.498	0.541	0.459
G (−40 V/ −75 V)	19.9	4.00	22.5	3.24	10	**−3.056**	2.101	2.931	0.526	0.474
G (−75 V/ −100 V)	22.5	3.24	24.8	4.84	10	**−2.559**	2.101	2.463	0.518	0.482
G (−40 V/ −100 V)	19.9	4.00	24.8	4.84	10	**−5.212**	2.101	4.997	0.539	0.461

as indicated by the statistic analysis, general averages (and standard deviations) for the nine samples deposited on the same condition can be calculated, resulting in 2.6 ± 0.52 N for the homogeneous samples and 2.5 ± 0.69 N for the graded samples. The statistical analysis between these two averages leads to accepting the null hypothesis, with a power of 75.8%. Therefore it is concluded that this quantity is not affected by the deposition mode, as well.

On the other hand, an increase in the average values of Lc2 for homogeneous and graded samples for all investigated bias is observed, but this increase can be considered significant only for the –100 V bias cases. The comparisons for –40 V and –75 V bias, although not significant (Table 12), are characterized by low powers (respectively 45.9% and 51.6%). Comparing samples grown by the same deposition mode under different bias, only the difference between averages of the –75 V and –100 V graded samples becomes statistically significant. As it was done for the critical interfacial shear strength and for Lc1, Lc2 was assumed to be independent on the bias, and general averages (and standard deviations) for the homogeneous and graded samples was calculated for the groups of nine samples, resulting in 2.96 ± 0.29 N for the homogeneous samples and 3.43 ± 0.14 N for the graded samples. The statistical analysis show that this difference is significant, and therefore, allows to conclude that the grade samples present improved cohesive properties.

3.4.2. Statistical analysis

Tables 11 and 12 present the analyses of the comparison for the Lc1 and Lc2 loads observed in the nanoscratching test. In the case of the Lc1 the null hypothesis is rejected only in the comparison between the homogeneous and grade films for –75 V bias, and for the graded films in the comparisons between –40 V and –75 V bias for the grade films. Both cases are affected by the low value of Lc1 for the graded samples produced under –75 V bias. The remaining cases suggest that Lc1 is independent both from the deposition mode and applied bias. This conclusion is reinforced by large values of power in some comparisons. As done in the case of the critical interfacial shear strength, a general average (and variance) for the nine samples corresponding to each deposition mode were calculated and the statistical test (last line of the table) confirms that both are to be considered identical, with a power of 75.8%.

Table 10
Results of the nanoscratching tests (uncertainties are estimated as the standard deviation of the measurements).

Condition	Lc1 [N]	Lc2 [N]
Homogeneous, –40 V bias	2.85 ± 0.28	3.11 ± 0.39
Homogeneous, –75 V bias	2.46 ± 0.14	2.81 ± 0.32
Homogeneous,–100 V bias	2.48 ± 0.21	2.97 ± 0.15
Graded, –40 V bias	2.95 ± 0.29	3.53 ± 0.17
Graded, –75 V bias	2.16 ± 0.02	3.30 ± 0.07
Graded,–100 V bias	2.50 ± 0.58	3.47 ± 0.04

Finally, the analysis of Lc2 apparently also shows an independence of this quantity from the process parameters, but in this case, it is observed that the three cases studied in which the graded samples are compared with the homogeneous ones this is followed by an increase in Lc2. As it was done for the critical interfacial shear strength, this allows us to obtain general averages for all 9 samples for each deposition mode which are represented in the last line of the Table 12. This shows that the graded films present a higher value of Lc2, which is consistent with a better adhesive performance compared with the homogeneous films. Since this is a single-tailed analysis, this conclusion is met with a confidence level corresponding to $\alpha = 0.025$.

4. Conclusions

The present work compared the properties of graded TiN films produced by grid-assisted magnetron sputtering with homogeneous TiN films produced in identical conditions.

GIXRD results indicate a change on preferred orientation depending on the deposition mode (either homogeneous of graded). The average compressive residual stresses in the homogeneous film, are similar, independent on the bias and range from -5 to -8 GPa.

Tensile tests allowed to estimate the critical interface shear strength, which is found to be independent on the bias, but dependent on the deposition mode. The critical interface shear strength was measured for the homogeneous films, resulting in 6.7 ± 2.2 GPa, and in 4.6 ± 0.7 GPa for the graded films.

Nanoindentation tests suggest that the Young modulus, E, is subject

Table 9
Statistical analysis for the γ parameter of the films as a function of deposition mode and of bias.

Comparison	Av1	Va1	Av2	Va2	n	t	$T_{0.05}^{2n-2}$	δ	$\beta = F_{\delta}^{2n-2}(t)$	1-β
−40 V (H/G)	0.23	0.0004	0.19	0.0016	10	**2.828**	2.101	2.856	0.472	0.528
−75 V (H/G)	0.19	0.0004	0.29	0.0025	10	**−5.872**	2.101	6.119	0.403	0.597
−100 V (H/G)	0.30	0.0009	0.33	0.0036	10	−1.414	2.101	1.428	0.482	**0.518**
H (−40 V/ −75 V)	0.23	0.0004	0.19	0.0004	10	**4.472**	2.101	4.283	0.538	0.462
H (−75 V/ −100 V)	0.19	0.0004	0.30	0.0009	10	**−9.648**	2.101	9.424	0.511	0.489
H (−40 V/ −100 V)	0.23	0.0004	0.30	0.0009	10	**−6.139**	2.101	5.997	0.509	0.491
G (−40 V/ −75 V)	0.19	0.0016	0.29	0.0025	10	**−4.938**	2.101	4.759	0.529	0.471
G (−75 V/ −100 V)	0.29	0.0025	0.33	0.0036	10	−1.620	2.101	1.558	0.510	**0.490**
G (−40 V/ −100 V)	0.19	0.0016	0.33	0.0036	10	**−6.139**	2.101	5.997	0.509	0.491

Table 11
Statistical analysis for the Lc1 load of the films as a function of deposition mode and of bias.

Comparison	Av1	Va1	Av2	Va2	n	t	$T_{0.05}^{2n-2}$	δ	$\beta = F_{\delta}^{2n-2}(t)$	1-β
−40 V (H/G)	2.85	0.0784	2.95	0.0841	3	−0.430	2.776	0.344	0.294	**0.706**
−75 V (H/G)	2.46	0.0196	2.16	0.0004	3	**3.674**	2.776	3.674	0.433	0.567
−100 V (H/G)	2.48	0.0441	2.5	0.3364	3	−0.056	2.776	0.050	0.0420	**0.958**
H (−40 V/ −75 V)	2.85	0.0784	2.46	0.0196	3	2.158	2.776	4.994	0.368	**0.632**
H (−75 V/ −100 V)	2.46	0.0196	2.48	0.0441	3	−0.137	2.776	1.110	0.415	**0.585**
H (−40 V/ −100 V)	2.85	0.0784	2.48	0.0441	3	1.831	2.776	1.014	0.518	**0.482**
G (−40 V/ −75 V)	2.95	0.0841	2.16	0.0004	3	**4.610**	2.776	1.820	0.561	0.439
G (−75 V/ −100 V)	2.16	0.0004	2.5	0.3364	3	−1.045	2.776	0.112	0.102	**0.898**
G (−40 V/ −100 V)	2.95	0.0841	2.5	0.3364	3	1.236	2.776	1.480	0.575	**0.425**
H/G	2.60	0.2700	2.5	0.4700	9	0.332	2.120	0.329	0.242	**0.758**

Table 12
Statistical analysis for the Lc2 load of the films as a function of deposition mode and of bias.

Comparison	Av1	Va1	Av2	Va2	n	t	$T_{0.05}^{2n-2}$	δ	$\beta = F_{\delta}^{2n-2}(t)$	1-β
−40 V (H/G)	3.11	0.1521	3.53	0.0289	3	−1.710	2.776	1.470	0.541	**0.459**
−75 V (H/G)	2.81	0.1024	3.30	0.0049	3	−2.591	2.776	2.462	0.484	**0.516**
-100 V (H/G)	2.97	0.0225	3.47	0.0016	3	**del-−5.579**	2.776	5.157	0.497	0.503
H (−40 V/ −75 V)	3.11	0.1521	2.81	0.1024	3	1.030	2.776	0.828	0.507	**0.493**
H (−75 V/ −100 V)	2.81	0.1024	2.97	0.0225	3	−0.784	2.776	0.667	0.439	**0.561**
H (−40 V/ −100 V)	3.11	0.1521	2.97	0.0225	3	0.580	2.776	0.508	0.364	**0.636**
G (−40 V/ −75 V)	3.53	0.0289	3.30	0.0049	3	2.167	2.776	1.878	0.545	**0.455**
G (−75 V/ −100 V)	3.30	0.0049	3.47	0.0016	3	**−3.652**	2.776	3.028	0.587	0.413
G (−40 V/ −100 V)	3.53	0.0289	3.47	0.0016	3	0.595	2.776	0.560	0.363	**0.637**
H/G	2.96	0.0841	3.43	0.0196	9	**−4.379**	2.120	4.416	0.464	0.536

to a statistical scatter of unknown origin. An indicative value of 240 GPa was estimated based on the data. Film hardness, *H*, has a trend to increase with the applied bias, both in the homogeneous and in the graded films. The film toughness, estimated from the indentation tests using the γ parameter, is also found to increase with the bias, and it is larger in the graded samples (at least the ones obtained with –75 V and –100 V bias).

Nanoscratching tests identified no clear dependence of the critical load for cohesive failure (Lc1) both on the bias and on the deposition mode, but the critical load for film delamination (Lc2) is definitely increased from 2.96 ± 0.29 N in the homogeneous samples to 3.43 ± 0.14 N in the case of the graded samples, which suggest that film adhesion is greater in the case of the graded films.

The results herein reported show graded films have superior adhesive properties, compared with the homogeneous films.

Funding sources

The present work was funded by the Brazilian National Research, Technology and Innovation Council (CNPq, Brasília, Brazil) under project 312424/2013-2 and by the São Paulo State Research Funding Foundation (FAPESP, São Paulo, Brazil) under project 2016/05768-2. This project was partially funded by the Santa Catarina state research funding agency (FAPESC) through the program PAP in association with the Santa Catarina State University under contract PAP-TR 655. MAT is grateful for a previous funding support from ASTRO, a United States Department of Energy workforce development program implemented at Oak Ridge National Laboratory through the Oak Ridge Institute for Science and Education under contract DE-AC05-06OR23100.

CRediT authorship contribution statement

Felipe C. Silva: Investigation, Methodology, Writing - original draft. **Matheus A. Tunes:** Methodology, Supervision, Resources, Writing - review & editing. **Julio C. Sagás:** Methodology, Supervision, Resources, Writing - review & editing. **Luis C. Fontana:** Methodology, Supervision, Resources, Writing - review & editing. **Nelson B. de Lima:** Methodology, Supervision, Resources, Writing - review & editing. **Cláudio G. Schön:** Conceptualization, Supervision, Project administration, Funding acquisition, Writing - review & editing.

Declaration of Competing Interest

The authors declare that they have no known competing financial interests or personal relationships that could have appeared to influence the work reported in this paper.

References

[1] M. Ohring, The Materials Science of Thin Films, Academic Press, Hoboken-NJ, 2002.
[2] J. Gerth, U. Wiklund, The influence of metallic interlayers on the adhesion of PVD TiN coatings on high-speed steel, Wear 264 (2008) 885–892.
[3] F.F. Komarov, V.M. Konstantinov, A.V. Kovalchuk, S.V. Konstantinov, H.A. Tkachenko, The efect of steel substrate pre-hardening on structureal, mechanical and tribological properties of magnetron sputtered TiN and TiAlN coatings, Wear (2016) 92–101. 352–353
[4] C.Y.H. Lim, S.C. Lim, K.S. Lee, The performance of TiN-coated high speed steel tool inserts in turning, Tribol. Int. 32 (1999) 393–398.
[5] B. Beake, V. Vishnyakov, A. Harris, Nano-scratch testing of (Ti, Fe) N_x thin films on silicon, Surf. Coat. Technol. 309 (2017) 671–679.
[6] C. Kainz, N. Schalk, M. Tkadletz, C. Mitterer, C. Czettl, Microstructure and mechanical properties of CVD TiN/TiBN multilayer coatings, Surf. Coat. Technol. 370 (2019) 311–319.
[7] C. Kainz, N. Schalk, M. Tkadletz, C. Mitterer, C. Czettl, The effect of b and c addition on microstructure and mechanical properties of TiN hard coatings grown by chemical vapor deposition, Thin Solid Films 688 (2019) 137213.
[8] N.K. Ponon, D.J.R. Appleby, E. Arac, P.J. King, S. Ganti, K.S.K. Kwa, A. O'Neill, Effect of deposition conditions and post-deposition anneal on reactivelly sputtered titanium nitride thin films, Thin Solid Films 578 (2015) 31–37.
[9] G. Zhao, T. Zhang, T. Zhang, J. Wang, G. Han, Electrical and optical properties of titanium nitride coatings prepared by atmospheric pressure chemical vapor deposition, J. Non-Cryst. Solids 354 (2008) 1272–1275.
[10] M. Elmkhah, F. Attarzadeh, A. Fattah-Al Hosseini, K.H. Kim, Microstructure and electrochemical comparisson between TiN coatings deposited through HIPIMS and DCMS techniques, J. Alloys Comp. 735 (2018) 422–429.
[11] R.D. Arnell, J.S. Colligon, K.F. Minnebaev, V.E. Yurasova, The effect of nitrogen content on the structural and mechanical properties of TiN films produced by sputtering, Vacuum 47 (1996) 425–431.
[12] S. Zhang, W. Zhu, TiN coating of tool steels: a review, J. Mater. Proc. Tech. 39 (1993) 165–177.

[13] E. Alat, A.T. Motta, R.J. Comstock, J.M. Partezana, D.E. Wolfe, Ceramic coating for corrosion (c3) resistance of nuclear fuel cladding, Surf. Coat. Technol. 281 (2015) 133–143.
[14] E. Alat, A.T. Motta, R.J. Comstock, J.M. Partezana, D.E. Wolfe, Multilayer (TiN, TiAlN) ceramic coatings for nuclear fuel cladding, J. Nucl. Mater. 478 (2016) 236–244.
[15] M.A. Tunes, F.C. Silva, O. Camara, C.G. Schön, J.C. Segás, L.C. Fontana, S.E. Donnelly, G. Greaves, P.D. Edmondson, Energetic particle irradiation study of TiN coatings: are these films appropriate for accident tolerant fuels? J. Nucl. Mater. 512 (2018) 239–245.
[16] A. Kozlovskiy, M. Abdigaliyev, G. Akhtanova, M. Zdorovets, Radiation resistance of thin TiN films as a result of irradiation with low-energy kr14+ ions, Ceram. Int. 46 (6) (2020) 7970–7976.
[17] W. Ming'e, M. Guojia, L. Xing, D. Chuang, Morphology and mechanical properties of TiN coatings prepared with different PVD methods, Rare Met. Mater. Eng. 45 (12) (2016) 3080–3084.
[18] P.J. Kelly, R.D. Arnell, Magnetron sputtering: a review of recent developments and applications, Vacuum 56 (3) (2000) 159–172.
[19] L. Fontana, J. Muzart, Characteristics of triode magnetron sputtering: the morphology of deposited titanium films, Surf. Coatings Technol. 107 (1998) 24–30.
[20] L.C. Fontana, J.L.R. Muzart, Triode magnetron sputtering TiN film deposition, Surf. Coat. Technol. 114 (1999) 7–12.
[21] J.C. Sagás, L.C. Fontana, H.S. MacIel, Influence of electromagnetic confinement on the characteristics of a triode magnetron sputtering system, Vacuum 85 (2011) 705–710.
[22] J.C. Sagás, D.a. Duarte, S.F. Fissmer, Effect of oxygen concentration and system geometry on the current-voltage relations during reactive sputter deposition of titanium dioxide thin films, Vacuum 85 (2011) 1042–1045.
[23] J.C. Sagás, D.A. Duarte, L.C. Fontana, Unusual behaviour of currentvoltage relations in an unbalanced grid-assisted magnetron sputtering system, J. Phys. D. Appl. Phys. 45 (2012) 505204.
[24] J. Sagás, R. Pessoa, H. Maciel, Langmuir probe measurements in a grid-assisted magnetron sputtering system, Braz. J. Phys. 48 (1) (2018) 61–66.
[25] J.C. Sagás, D.a. Duarte, D.R. Irala, L.C. Fontana, T.R. Rosa, Modeling reactive sputter deposition of titanium nitride in a triode magnetron sputtering system, Surf. Coatings Technol. 206 (2011) 1765–1770.
[26] A.J. Perry, V. Valvoda, D. Rafaja, X-Ray residual stress measurement in TiN, ZrN and HfN films using the Seemann-Bohlin method, Thin Solid Films 214 (2) (1992) 169–174.
[27] M. Benegra, D. Lamas, M.F. de Rapp, N. Mingolo, A. Kunrath, R.M. Souza, Residual stresses in titanium nitride thin films deposited by direct current and pulsed direct current unbalanced magnetron sputtering, Thin Solid Films 494 (1–2) (2006) 146–150.
[28] A. Gómez, A.A.C. Recco, N. Lima, L. Martinez, A.P. Tschiptschin, R. Souza, Residual stresses in titanium nitride thin films obtained with step variation of substrate bias voltage during deposition, Surf. Coatings Technol. 204 (20) (2010) 3228–3233.
[29] F.C. da Silva, M.A. Tunes, P.D. Edmondson, N.B. Lima, J. Segás, L.C. Fontana, C.G. Schön, Grid-assisted magnetron sputtering deposition of nitrogen graded TiN thin films, SN Appl. Sci. 2 (5) (2020) 865.
[30] M. Van Stappen, B. Malliet, L. De Schepper, L.M. Stals, J.P. Celis, J.R. Roos, Influence, of Ti intermediate layer on properties of TiN coatings deposited on various substrates, Surf. Eng 5 (4) (1989) 305–310.
[31] L. De Schepper, M. D'Olieslaeger, G. Knuyt, L.M. Stals, M. Van Stappen, B. Malliet, J.P. Celis, J.R. Roos, Initial growth and epitaxy of PVD TiN layers on austenitic steel, Thin Solid Films 173 (2) (1989) 199–208.
[32] C. Quaeyhaegens, L.M. Stals, M. Van Stappen, L. De Schepper, Interface study of TiN- and ti-tin- coated stainless steel AISI 304 with asymmetric glancing angle x-ray diffraction and classical bragg-brentano x-ray diffraction, Thin Solid Films 197 (1991) 37–46.
[33] K. Strijckmans, R. Schelfhout, D. Depla, Tutorial: hysteresis during the reactive magnetron sputtering process, J. Appl. Phys. 124 (24) (2018) 241101.
[34] B.D. Cullity, S.R. Stock, Elements of X-ray diffraction, 3rd, Pearson, 2001.
[35] G.M. Pharr, W.C. Oliver, F.R. Brozen, On the generality of the relationship among contact stiffness, contact area, and elastic modulus during indentation, J. Mater. Res. 7 (1992) 613–617.
[36] R. Lupton, Statistics in theory and practice, Princeton University Press, 1993.
[37] G.J. Resnikoff, G.J. Lieberman, Table of the Non-Central t-Distribution, Technical Report 32, Office of Naval Research, Stanford, 1957.
[38] S. Mahieu, D. Depla, Reactive sputter deposition of TiN layers: modelling the growth by characterization of particle fluxes towards the substrate, J.Phys. D. Appl. Phys. 42 (5) (2009) 053002.
[39] F.C. da Silva, M.A. Tunes, J.C. Segás, C.G. Schön, Influence of substrate stiffness and of PVD parameters on the microstructure and tension fracture characteristics of TiN thin films, Procedia Struct. Integrity 13 (2018) 658–663.
[40] C.G. Schön, Mechanics of Materials, Elsevier, Rio de Janeiro, 2013.
[41] M.A. Meyers, K.K. Chawla, Mechanical behavior of materials, 1st, Prentice Hall, Upper Saddle River – NJ, 1999.
[42] D.C. Agrawal, R. Raj, Measurement of ultimate shear strength of a metal – ceramic interface, Acta Metall. 37 (1989) 1265–1270.
[43] J.-H. Jeong, D. Kwon, Evaluation of the adhesive strength in DLC film-coated systems evaluated by the film-cracking thechnique, J. Adhes. Sci. Tech. 12 (1998) 29–46.
[44] G. Pharr, Measurement of mechanical properties by ultra-low load indentation, Mater. Sci. Eng. A 253 (1998) 151–159.
[45] R.C. Cozza, A study on friction coefficient and wear coefficient of coated systems submitted to micro-scale abrasion tests, Surf. Coat. Technol. 215 (2013) 224–233.
[46] J. Musil, F. Kunc, H. Zeman, H. Poláková, Relationships between hardness, Young's modulus and elastic recovery in hard nanocomposite coatings, Surf. Coatings Technol. 154 (2–3) (2002) 304–313.